The current issue and full text archive of this journal is available at
www.emeraldinsight.com/0961-5539.htm

Received 3 April 2007
Revised 28 February 2008
Accepted 12 March 2008

Convective heat transfer augmentation through vortex shedding in sinusoidal constricted tube

J. Batina
L.A.T.E.P. Groupe Transferts Thermiques, Université de Pau et des Pays de l'Adour, Hélioparc Pau-Pyrénées, Pau, France
M. Batchi
L.A.T.E.P. Groupe Transferts Thermiques, Université de Pau et des Pays de l'Adour, Hélioparc Pau-Pyrénées, Pau, France and Laboratoire de Mathématiques Appliquées, Université de Pau et des Pays de l'Adour, Pau, France
S. Blancher and R. Creff
L.A.T.E.P. Groupe Transferts Thermiques, Université de Pau et des Pays de l'Adour, Hélioparc Pau-Pyrénées, Pau, France, and
C. Amrouche
Laboratoire de Mathématiques Appliquées, Université de Pau et des Pays de l'Adour, Pau, France

Abstract

Purpose – The purpose of this paper is to analyse the convective heat transfer of an unsteady pulsed, laminar, incompressible flow in axisymmetric tubes with periodic sections. The flow is supposed to be developing dynamically and thermally from the duct inlet. The wall is heated at constant and uniform temperature.

Design/methodology/approach – The problem is written with classical homogeneous boundary conditions. We use a shift operator to impose non-homogeneous boundary conditions. Consequently, this method introduces source terms in the Galerkin formulation. The momentum equations and the energy equation which govern this problem are numerically solved in space by a spectral Galerkin method especially oriented to this situation. A Crank-Nicolson scheme permits the resolution in time.

Findings – From the temperature field, the heat transfer phenomenon is presented, discussed and compared to those obtained in straight cylindrical pipes. This study showed the existence of zones of dead fluid that locally have a negative influence on heat transfer. Substantial modifications of the thermal convective heat transfer are highlighted at the entry and the minimum duct sections.

Practical implications – Pulsated flows in axisymmetric geometries can be applied to medical industries, mechanical engineering and technological processes.

Originality/value – One of the original features of this study is the choice of Chebyshev polynomials basis in both axial and radial directions for spectral methods, combined with the use of a shift operator to satisfy non-homogeneous boundary conditions.

Keywords Convection, Heat transfer, Flow, Thermodynamics
Paper type Research paper

Nomenclature

a	thermal diffusity: $a = k/\rho c_p (\mathrm{m}^2/\mathrm{s})$	h	wall function
c_p	thermal capacity (J/Kg.K)	h_T	convective heat transfer coefficient ($\mathrm{W/m^2K}$)
e	reduced amplitude		

International Journal of Numerical Methods for Heat & Fluid Flow
Vol. 19 Nos. 3/4, 2009
pp. 374-395
© Emerald Group Publishing Limited
0961-5539
DOI 10.1108/09615530910938335

H	periodic sinusoidal radius (m)
k	heat conductivity (W/m.K)
L	geometric half-period tube (m)
p	pressure (N/m^2)
R	tube radius at the constriction (m)
r	radial co-ordinate (m)
T	fluid temperature (K)
T_W	wall temperature (K)
T_∞	duct inlet temperature (K)
t	time (s)
$\bar{t}_0$	dimensionless time: $\bar{t}_0 = L/\bar{u}_0$
$\vec{V} = (u, v)$	velocity field
u	axial velocity (m/s)
$\bar{u}_0$	mean bulk velocity (m/s)
v	radial velocity (m/s)
z	axial co-ordinate (m)

Greek symbols

Φ_W	wall heat flux (W/m^2)
λ	dimensionless wavelength
θ	dimensionless temperature: $\theta = (T - T_\infty)/(T_W - T_\infty)$
μ	dynamic viscosity (Ns/m^2)
ν	kinematic viscosity: $\nu = \mu/\rho$(m^2/s)
ρ	fluid density (Kg/m^3)
τ	modulation flow rate
$\bar{\omega}_0$	vorticity function reference (1/s) $\bar{\omega}_0 = \bar{u}_0/R$
$\bar{\psi}_0$	stream function reference (m^3/s) $\bar{\psi}_0 = \bar{u}_0 R^2$
Ω	pulsation (rad/s)

Dimensionless numbers

Re	Reynolds number based on the radius at the constriction: $\mathrm{Re} = R\bar{u}_0/\nu$
Pr	Prandtl number: $\mathrm{Pr} = \nu/a$
Nu	Nusselt number
$\theta_{0m}(x)$	averaged bulk temperature

Subscripts

0	steady flow
W	wall

1. Introduction

In order to obtain convective heat transfer enhancement, most of the studies are linked to:

(1) Firstly, the search for optimal geometries (undulated or grooved channels, tube with periodic sections, etc. . . .): among those geometrical studies, with constant flow, one can quote the investigations of Blancher (1991), Ghaddar *et al.* (1986), for the wavy or grooved plane geometries, in order to highlight the influence of the forced or natural disturbances on heat transfer.

(2) Secondly, the search for particular flow conditions (transient regime, pulsed flow, etc.): for example those linked to the periodicity of the pressure gradient (Chakravarty and Sannigrahi, 1999; Hemida *et al.*, 2002; Batina, 1995), or those which impose a periodic velocity condition (Young Kim *et al.*, 1998; Lee *et al.*, 1999) or those which carry on time periodic deformable walls.

Pulsed ducted unsteady flow in a simple axisymmetric geometry has been intensively investigated, using theoretical models or experimental tests. One could notice works concerning unsteady axisymmetric ducted flows, laminar or turbulent, in cylindrical geometry whose analysis has been made by the use of asymptotic methods (Creff *et al.*, 1985; André *et al.*, 1981, 1987; Batina *et al.*, 1991, 1989). The aim of those studies was to

quantify particular flow conditions, as Reynolds number, frequency, geometrical parameters which give high convective heat transfer, under constant heat flux or uniform wall temperature hypothesis.

We can mention Moschandreau and Zamir (1997) studies, which examine the effects of pulsation on heat transfer when the field velocity is described in term of superposition of an established Poiseuille profile and an unsteady pulsatile velocity component. They show that under those hypotheses there is an enhancement or reduction of heat transfer when walls are heated at uniform temperature. They observed that for non-dimensional frequency around to 15, there is an increase in the fluid average temperature as well as thermal heat transfer.

The pulsated flows studies also highlighted the blood circulation behaviours in arteries presenting some stenosis or constrictions. From a medical point of view, those constrictions arteries are responsible for vascular system diseases. For example, Ryval *et al.* (2003), Guo-Tao *et al.* (2004), Gurek *et al.* (2002), studied a laminar blood circulation in the vicinity of two consecutive constrictions in a vascular tube for Reynolds numbers located between 25 and 1,000. They conclude that the flow in the arterial model is influenced by the Reynolds number, the height of stenosis and the geometry of constrictions.

Those types of pulsated flows are also found in many applications such as medical biology, industrial engineering and other technological processes (Fedele *et al.*, 2005; Chakravarty and Sannigrahi, 1999). Different works of those authors as Fedele *et al.* (2005) show that it is necessary to build a model taking into account physical, geometrical and temporal flow characteristics.

There are few works relating to the study of the pulsated flows in complex geometries and in particular axisymmetric geometries with periodic section. In this paper, we will study this particular case searching for optimal flow conditions which lead to heat transfer increase. We will compare at least the present numerical resolution to the cylindrical geometry case (see for example the previous studies of Creff *et al.* (1985)).

From a numerical point of view, the Navier-Stokes equations written in $(\omega - \psi)$ formulation and the energy equation are solved in space by spectral Galerkin methods (Canuto *et al.*, 1988; Bernardi and Maday, 1992; Gelfgat, 2004; Shen, 1994, 1995, 1997). Those classic methods are largely used to solve partial differential equations. The resolution in time is carried out by Crank-Nicolson scheme.

This work can be summarised as follows: in the first section, we give governing equations and boundary conditions associated to the physical model. Next, we describe the spectral numerical method to solve these equations. Then the numerical studies focus on the thermal problem and its associated heat transfer. Finally, in the last section, numerical results obtained are analysed in the following order: study of the dynamic field – evolution of the temperature field – thermal heat transfer. A discussion is given in conclusion.

2. Hypotheses and governing equations

2.1 Hypotheses

We consider a Newtonian incompressible fluid flow developing inside an axisymmetric cylindrical duct with periodic sinusoidal radius. The unsteadiness imposed to the flow corresponds to a source of periodic pulsations generating plane waves. This flow is described in terms of an unsteady pulsed flow superimposed on a steady one. With regard to the thermal problem, the wall is heated at constant and uniform temperature, and the fluid inlet temperature for the steady regime is equal to the upstream ambient temperature. Physical properties of the fluid are supposed to be independent of the temperature, which involves that the motion and energy equations are uncoupled.

The geometry of the domain is given by Figure 1 where we consider n_0 geometrical periods.

2.2 Governing equations

The Navier-Stokes governing equations are:

$$\frac{\partial \vec{V}}{\partial t} + (\vec{V} \cdot \vec{\nabla})\vec{V} = -\frac{1}{\rho}\vec{\nabla}p + \nu\nabla^2\vec{V} \tag{1}$$

$$\vec{\nabla} \cdot \vec{V} = 0 \tag{2}$$

The energy equation is:

$$\frac{\partial T}{\partial t} + (\vec{V} \cdot \vec{\nabla})T = a\Delta T \tag{3}$$

With the 2D hypothesis, we use the vorticity-stream function formulation (ω, ψ) for the Navier-Stokes equations in which the incompressibility condition is automatically satisfied. In fact, the essential advantage of this formulation compared to the primitive variables (velocity–pressure formulation) is the reduction of the number of unknown functions and the non-used of the pressure. But this ψ equation becomes a fourth order partial differential equation.

3. Boundary conditions

The present problem is unsteady. This unsteadiness is generated at the initial instant $t = 0$, and is sustained during all the time by a source of upstream pulsations. Before that instant, we consider that the flow is steady. Because of a scheme in time used, it is necessary for us to solve the steady problem first. Thus, the obtained solution is introduced as initial condition in the unsteady problem. The boundary conditions are therefore of two types: boundary conditions for the steady flow (without pulsation) and boundary conditions for the unsteady flow. They can be summarised as follow:

3.1 Steady flow ($t = 0$ time step)

- *Entry*: for the dynamic problem, Poiseuille profile boundary condition is chosen $u_0(z = 0, r) = 2\bar{u}_0\left(1 - (r/R)^2\right)$.
- For the thermal problem, the inlet fluid temperature is equal to the upstream ambient temperature: $T = T_\infty$.

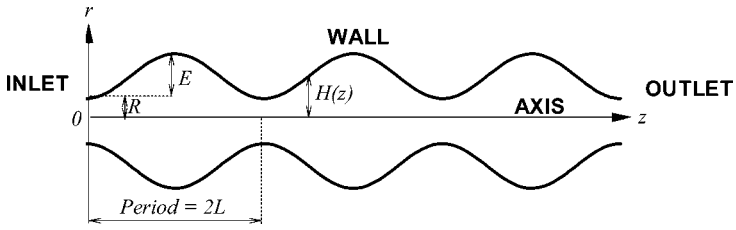

Figure 1.
Geometry domain study

- *Exit*: the flow velocity is normal to the exit section and verifies the classical flow condition $v_0 = 0$ and $\partial T_0/\partial z = \partial u_0/\partial z = 0$.
- *Axis*: axial symmetry: $\partial u/\partial r = v = \partial T/\partial r = 0$.
- *Wall*: slip condition is imposed and the wall heated at constant temperature: $u = v = 0; T = T_W$.

3.2 Unsteady flow $(t > 0)$

- *Entry*: the source of pulsations at the entry section imposes a periodic pressure gradient modulation. Then the velocity axial component and the stream function ψ have a Fourier series expansion in time, such as: $f(z = 0, r, t) = f_0(z = 0, r)\left(1 + \sum_{n=1}^{N_F} \tau^n . sin(n\Omega)\right)$

where f represents u or ψ.

At this section, to avoid reverse flow, we impose: $\tau < 1$.

- *Exit*: conditions similar to steady flow exit conditions: $v = 0$ and $\partial T/\partial z = \partial u/\partial z = 0$.
- *Axis*: the flow preserves at each time an axial symmetry: $\partial u/\partial r = v = \partial T/\partial r = 0$.
- *Wall*: conditions similar to steady flow wall conditions: $u = v = 0; T = T_W$.

4. Resolution of the dynamic problem

4.1 The (ω, ψ) *formulation*

The momentum equation is explicitly written in (ω, ψ) formulation, such as:

$$\frac{\partial \hat{\omega}}{\partial t} - \frac{1}{r}\frac{\partial \psi}{\partial z}\frac{\partial \hat{\omega}}{\partial r} + \frac{1}{r}\frac{\partial \psi}{\partial r}\frac{\partial \hat{\omega}}{\partial z} + \frac{2}{r^2}\frac{\partial \psi}{\partial z}\hat{\omega} = \nu\left(\frac{\partial^2 \hat{\omega}}{\partial r^2} + \frac{\partial^2 \hat{\omega}}{\partial z^2} - \frac{1}{r}\frac{\partial \hat{\omega}}{\partial r}\right) = \nu\Delta\hat{\omega} \quad (4)$$

$$\hat{\omega} = r\omega = -\left(\frac{\partial^2 \psi}{\partial r^2} + \frac{\partial^2 \psi}{\partial z^2} - \frac{1}{r}\frac{\partial \psi}{\partial r}\right) = \Delta\psi \quad (5)$$

4.2 New formulation of the problem

4.2.1 Dimensionless quantities and variables transformations. One chooses for reference variables:

$$\widetilde{r} = \frac{r}{R}; \widetilde{z} = \frac{z}{R}; \widetilde{t} = \frac{t}{\bar{t}_0}; \widetilde{\omega} = \frac{\hat{\omega}}{\bar{\omega}_0}; \widetilde{\psi} = \frac{\psi}{\bar{\psi}_0} \quad (6)$$

with

$$\bar{t}_0 = \frac{L}{\bar{u}_0}; \bar{\omega}_0 = \frac{\bar{u}_0}{R}; \bar{\psi}_0 = \bar{u}_0 R^2 \quad (7)$$

For the thermal problem, the temperature $\widetilde{\theta}$ is made dimensionless in a classic way:

$$\widetilde{\theta} = \frac{T - T_\infty}{T_W - T_\infty} \tag{8}$$

For convenient reasons, the Reynolds number *Re* is based on the radius at the duct constriction:

$$\mathrm{Re} = \frac{R\bar{u}_0}{\nu} \tag{9}$$

In order to obtain a computational square domain permitting the use of two-dimensional Chebyshev polynomials, we proceed to a space variables transformation. This one is inspired by Sobey, and modified by Blancher. It has been adapted to the axisymmetric geometry used in this study. Afterwards, we note by $H(z)$ the duct periodic radius and by λ the duct wavelength. Then we define:

$$\rho = \frac{\widetilde{r}}{h(x)}; x = \frac{\widetilde{z}}{\lambda} - 1 \tag{10}$$

with:

$$\lambda = \frac{L}{R}; h(x) = \frac{1}{R}H[(x+1).L]; \tag{11}$$

and

$$H(z) = R\left\{1 + \frac{e}{2}\left[1 - \cos\left(\pi \,.\, n_O \frac{z}{L}\right)\right]\right\} \Leftrightarrow h(x) = 1 + \frac{e}{2}[1 - \cos(\pi \,.\, n_O(x+1))] \tag{12}$$

Finally, the study domain is transformed into a rectangle $-1 \le x \le 1$ and $0 \le \rho \le 1$ representing the half- space of the square:$[-1, 1] \times [-1, 1]$.

4.2.2 New system of governing equations. Considering the transformation of variables defined before, the new stream – vorticity formulation of this problem is:

$$\begin{cases} \breve{\omega} = -\Delta_f \widetilde{\psi} \\ h^2 \dfrac{\partial \breve{\omega}}{\partial \widetilde{t}} + \dfrac{1}{\rho}\left(\dfrac{\partial \widetilde{\psi}}{\partial \rho}\dfrac{\partial \breve{\omega}}{\partial x} - \dfrac{\partial \widetilde{\psi}}{\partial x}\dfrac{\partial \breve{\omega}}{\partial \rho}\right) + \dfrac{2}{\rho^2}\left(\dfrac{\partial \widetilde{\psi}}{\partial x} - 2\rho\dfrac{h'}{h}\dfrac{\partial \widetilde{\psi}}{\partial \rho}\right)\breve{\omega} \\ = \dfrac{1}{\widetilde{R}\,e}\Delta_g \breve{\omega} \end{cases} \tag{13}$$

where:

$$\Delta_f \widetilde{\psi} = \left\{ h^2 \frac{\partial^2 \widetilde{\psi}}{\partial x^2} - 2\rho h' h \frac{\partial^2 \widetilde{\psi}}{\partial x \partial \rho} + \left[\lambda^2 + \rho^2 h'^2\right]\frac{\partial^2 \widetilde{\psi}}{\partial \rho^2} + \left[\rho\left(2h'^2 - hh''\right) - \frac{\lambda^2}{\rho}\right]\frac{\partial \widetilde{\psi}}{\partial \rho}\right\} \tag{14}$$

and

$$\breve{\omega} = \lambda^2 h^2 \tilde{\omega}; \Delta_g \breve{\omega} = -\left\{ \begin{array}{l} A_g(x,\rho)\dfrac{\partial^2 \breve{\omega}}{\partial x^2} + B_g(x,\rho)\dfrac{\partial^2 \breve{\omega}}{\partial \rho^2} + C_g(x,\rho)\dfrac{\partial \breve{\omega}}{\partial \rho} \\ +D_g(x,\rho)\dfrac{\partial^2 \breve{\omega}}{\partial x \partial \rho} + E_g(x,\rho)\dfrac{\partial^2 \breve{\omega}}{\partial x} + F_g(x,\rho)\breve{\omega} \end{array} \right\} \tag{15}$$

with:

$$\left\{ \begin{array}{l} A_g(x,\rho) = h^2; B_g(x,\rho) = \lambda^2 + \rho^2 h'^2; C_g(x,\rho) = \rho\left(6h'^2 - hh''\right) - \dfrac{\lambda^2}{\rho}; \\ D_g(x,\rho) = -2\rho hh'; E_g(x,\rho) = -4hh'; F_g(x,\rho) = 2\left(3h'^2 - hh''\right) \end{array} \right. \tag{16}$$

$$\widehat{Re} = \widetilde{Re}\lambda^2 = Re\lambda \tag{17}$$

For reason of convenience, the radius ρ will be noted r as follows.

5. Numerical resolution of the dynamic problem

The spectral Galerkin method consists in projecting the unknown functions on polynomial basis of Chebyshev or Legendre (Canuto *et al.*, 1988; Bernardi and Maday, 1992). We will choose the Chebyshev polynomials, and study the influence of the physical parameters such as the Reynolds number (between 1 and 50) to remain in 2D hypothesis. From a numerical point of view we will show the influence of the polynomials degrees particularly for the thermal problem.

5.1 Resolution of the steady problem

The steady problem is written as follows:

$$\left\{ \begin{array}{l} \breve{\omega} = -\Delta_f \widetilde{\psi} \\ \dfrac{1}{r}\left(\dfrac{\partial \widetilde{\psi}}{\partial r}\dfrac{\partial \breve{\omega}}{\partial x} - \dfrac{\partial \widetilde{\psi}}{\partial x}\dfrac{\partial \breve{\omega}}{\partial r}\right) + \dfrac{2}{r^2}\left(\dfrac{\partial \widetilde{\psi}}{\partial x} - 2r\dfrac{h'}{h}\dfrac{\partial \widetilde{\psi}}{\partial r}\right)\breve{\omega} = \dfrac{1}{\widehat{Re}}\Delta_g \breve{\omega} \end{array} \right. \tag{18}$$

5.1.1 The spectral Galerkin method. This problem is written with classical homogeneous boundary conditions. One of the originalities of this study is the use of a shift operator allowing the introduction of non-homogeneous boundary conditions. For this reason, the unknown stream function $\widetilde{\psi}_0(x,r)$ is written by mean of the Poiseuille stream function $\phi_0(r)$ corresponding to the Poiseuille velocity imposed at the duct entry as:

$$\widetilde{\psi}_0(x,r) = \psi_0(x,r) + \varphi_0(r) \tag{19}$$

where the stream function $\psi_0(x,r)$ verifies homogeneous boundary conditions in both directions x and r.

The Equation (18) becomes:

$$\frac{1}{r^2}\frac{\partial\psi_0}{\partial x}(\alpha(\omega)+\alpha_\Phi)+\frac{1}{r}\frac{\partial\psi_0}{\partial r}(\beta(\omega)+\beta_\Phi)+\frac{1}{r}\frac{\partial\varphi_0}{\partial r}\beta(\omega)-\frac{1}{\widehat{Re}}\gamma(\omega)=\frac{1}{\widehat{Re}}\gamma_\Phi-\frac{1}{r}\frac{\partial\varphi_0}{\partial r}\beta_\Phi \tag{20}$$

with:

$$\alpha(\omega)=2\omega-r\frac{\partial\omega}{\partial r};\alpha_\Phi=2\Phi-r\frac{\partial\Phi}{\partial r};\beta(\omega)=\frac{\partial\omega}{\partial x}-4\frac{h'}{h}\omega;\beta_\Phi=\frac{\partial\Phi}{\partial x}-4\frac{h'}{h}\Phi;$$
$$\gamma(\omega)=\Delta_g\omega;\gamma_\Phi=\Delta_g\Phi;$$

and $\Phi(x,r)=-\Delta_f\varphi_0(r)$.

The corresponding Galerkin method consists in projecting the discretized equations on a Chebyshev polynomials basis, taking into account the whole boundary conditions (see Canuto *et al.*, 1988). Then, the stream-function $\widetilde{\psi}_0$, truncated at development orders N_x according to the axis x and N_r according to the radius r, is projected on trial functions as follows:

$$\widetilde{\psi}_0(x,r)=\sum_{k=0}^{N_x}\sum_{l=0}^{N_r}\psi_{kl}P_{2l}(r)Q_k(x) \tag{21}$$

where $P_{2l}(r)$ and $Q_k(x)$ are polynomial basis constructed from Chebyshev polynomials.

Because of the symmetry property, $P_{2l}(r)$ will be an even function. To construct the basis $P_{2l}(r)$, we choose a linear combination of Chebyshev polynomials such as (see Shen, 1994, 1995, 1997; Gelfgat, 2004):

$$P_{2l}(r)=T_{2l}(r)-\frac{l+1}{l+2}T_{2(l+1)}(r)-T_{2(l+2)}(r)+\frac{l+1}{l+2}T_{2(l+3)}(r) \tag{22}$$

In the $Q_k(x)$ polynomial basis case, there is no parity according to the axial variable x. Then, the basis functions $Q_k(x)$ can be constructed as follows:

$$Q_k(x)=T_k(x)-\frac{(k+3)^2(k+1)}{(k+2)^2(k+2)}T_{k+1}(x)-\frac{k^2}{(k+2)^2}T_{k+2}(x)+\frac{(k+3)^2(k+1)}{(k+2)^2(k+2)}T_{k+3}(x) \tag{23}$$

We notice that the non-linear system obtained is solved by the Newton algorithm.

5.2 Resolution of the unsteady problem

From Equation (13), introducing the unknown ψ function such as: $\widetilde{\psi}(x,r,t)=\psi(x,r,t)+\varphi(r)A(t)$ and using the Equations (20), we define the operator in which the

unknown coefficients depend now on time:

$$L_\psi(x,r,t) = -\left(\frac{1}{r^2}\frac{\partial\psi}{\partial x}(\alpha(\omega)+\alpha_\Phi) + \frac{1}{r}\frac{\partial\psi}{\partial r}(\beta(\omega)+\beta_\Phi) + \frac{1}{r}\frac{\partial\varphi}{\partial r}\beta(\omega) - \frac{1}{\widehat{R}e}\gamma(\omega)\right) + \frac{1}{\widehat{R}e}\gamma_\Phi - \frac{1}{r}\frac{\partial\varphi}{\partial r}\beta_\Phi \tag{24}$$

Then the previous problem (13)-(16) can take the following form:

$$h^2\frac{\partial\breve{\omega}}{\partial t} = L_\psi(x,r,t) \tag{25}$$

where $\breve{\omega} = \omega + \omega_\Phi$ and the operator $L_\psi(x,r,t)$ is non-linear. Notice that ω_Φ is the contribution coming from Poiseuille extension.

The temporal discretization of (25) is made by using the ε-method, reduced here to Crank-Nicolson method. The advantage of this method is to be unconditionally stable. It leads to the equation below with $\varepsilon = 1/2$, which corresponds to a two order scheme:

$$\begin{cases} h^2\dfrac{\omega^{n+1}-\omega^n}{\Delta t} + h^2\dfrac{\partial\omega_\Phi(x,r,t)}{\partial t} = \varepsilon L_{\psi^{n+1}}(x,r,t) + (1-\varepsilon)L_{\psi^n}(x,r,t) \\ \omega^n = -\Delta_f\psi^n, \forall n \end{cases} \tag{26}$$

where the initial condition is given by the solution of the steady problem:

$$\psi_{kl}(t=0) = \psi^0_{kl} \tag{27}$$

The relation (23) has the form:

$$h^2\omega^{n+1} - \varepsilon L_{\psi^{n+1}}(x,r,t) = S_{\psi^n} \tag{28}$$

with

$$S_{\psi^n} = h^2\omega^n - h^2\Delta t\frac{\partial\omega_\Phi}{\partial t} + (1-\varepsilon)\Delta t L_{\psi^n}(x,r,t) \tag{29}$$

where

$$\omega_\Phi = \Phi(x,r)A(t) \text{ with } A(t) = \left(1 + \sum_{1\le p\le N_F}\tau^p\sin(p\Omega t)\right) \tag{30}$$

The unknowns $\psi_{kl}(t)$ are obtained by projecting on the same basis as for the steady situation before. At each time step, the non-linear system is solved by the Newton algorithm.

6. Numerical resolution of the thermal problem

6.1 Expression of the energy equation

Using (3) and (6)-(8), the dimensionless energy equation can be written as follows:

$$h^2\frac{\partial\widetilde{\theta}}{\partial\widetilde{t}} + h^2\widetilde{u}\frac{\partial\widetilde{\theta}}{\partial x} + h(\widetilde{v}\lambda - \widetilde{u}rh')\frac{\partial\widetilde{\theta}}{\partial r} = \frac{1}{\widehat{\mathrm{R}}\,\mathrm{ePr}}\Delta_f\widetilde{\theta} \tag{31}$$

with:

$$\Delta_f\widetilde{\theta} = h^2\frac{\partial^2\widetilde{\theta}}{\partial x^2} - 2rh'h\frac{\partial^2\widetilde{\theta}}{\partial x\partial r} + \left[\lambda^2 + r^2h'^2\right]\frac{\partial^2\widetilde{\theta}}{\partial r^2} + \left[r\left(2h'^2 - hh''\right) + \frac{\lambda^2}{r}\right]\frac{\partial\widetilde{\theta}}{\partial r} \quad (32)$$

6.2 Numerical resolution

6.2.1 Choices of the basis functions. The choice of the temperature basis functions is made in the same way as in the dynamic problem. In order to apply the Galerkin method, we consider the boundary conditions (section 3) for the temperature θ. Let us set $\widetilde{\theta}(x,r,t) = \theta(x,r,t) + \theta_R(r)$ where θ is the solution satisfying the homogeneous boundary conditions and $\theta_R(r)$ is a smoothed gap temperature imposed at the entry. The homogeneous temperature θ, truncated at development orders M_x according to the axis x and M_r according to the radius r, is projected on the trial functions as follows:

$$\theta(x,r,t) = \sum_{k=0}^{M_x}\sum_{l=0}^{M_r}\theta_{kl}(t)q_k(x)p_{2l}(r) \quad (33)$$

where $p_{2l}(r)$ and $q_k(x)$ are built from Chebyshev polynomials as in section 5. According to temperature boundary conditions as in section 3, we obtain, at last:

$$q_k(x) = T_k(x) + \frac{4(k+1)}{(k+1)^2 + (k+2)^2}T_{k+1}(x) - \frac{(k+1)^2 + k^2}{(k+1)^2 + (k+2)^2}T_{k+2}(x), \quad \text{if } 0 \le k \le M_x \quad (34)$$

and the polynomial $p_{2l}(r)$ is given by:

$$p_{2l}(r) = T_{2l}(r) - T_{2(l+1)}(r), \quad \text{if } 0 \le l \le M_r. \quad (35)$$

6.2.2 Resolution of the steady problem. With (19) and $\widetilde{\theta}(x,r) = \theta(x,r) + \theta_R(r)$, the steady thermal problem is written as follows:

$$\frac{1}{r}\frac{\partial\psi}{\partial r}\cdot\frac{\partial\theta}{\partial x} - \frac{1}{r}\frac{\partial\psi}{\partial x}\cdot\frac{\partial\theta}{\partial r} + 2(1-r^2)\frac{\partial\theta}{\partial x} - \frac{1}{\widehat{\mathrm{R}}\,\mathrm{ePr}}\Delta_f\theta = \frac{1}{r}\frac{\partial\psi}{\partial x}\cdot\frac{\partial\theta_R}{\partial r} + \frac{1}{\widehat{\mathrm{R}}\,\mathrm{ePr}}\Delta_f\theta_R \quad (36)$$

The system obtained is solved by a Gauss type classical method.

6.2.3 The unsteady problem resolution. The unsteady problem is written as follows:

$$\frac{\partial\theta}{\partial t} = -\frac{1}{h^2}\left(\frac{1}{r}\frac{\partial\psi}{\partial r}\cdot\frac{\partial\theta}{\partial x} - \frac{1}{r}\frac{\partial\psi}{\partial x}\cdot\frac{\partial\theta}{\partial r} + \frac{1}{r}\frac{\partial\varphi}{\partial r}\frac{\partial\theta}{\partial x} - \frac{1}{\widehat{\mathrm{R}}\,\mathrm{ePr}}\Delta_f\theta\right) + \frac{1}{h^2}\left(\frac{1}{r}\frac{\partial\psi}{\partial x}\cdot\frac{\partial\theta_R}{\partial r} + \frac{1}{\widehat{\mathrm{R}}\,\mathrm{ePr}}\Delta_f\theta_R\right) \quad \theta(x,r,0) = \theta_0(x,r) \quad (37)$$

where $\theta_0(x,r)$ is the steady thermal problem solution.

The Equation (37) is numerically integrated in time by using the second order Crank-Nicolson scheme ($\varepsilon = 1/2$) which is formulated as follows:

$$\frac{\theta^{n+1} - \theta^n}{\Delta t} = \varepsilon L_{\theta^{n+1}}(x, r, t) + (1 - \varepsilon) L_{\theta^n}(x, r, t) \tag{38}$$

where

$$L_\theta(x, r, t) = -\frac{1}{h^2}\left(\frac{1}{r}\frac{\partial\psi}{\partial r}\cdot\frac{\partial\theta}{\partial x} - \frac{1}{r}\frac{\partial\psi}{\partial x}\cdot\frac{\partial\theta}{\partial r} + \frac{1}{r}\frac{\partial\varphi}{\partial r}A(t)\frac{\partial\theta}{\partial x} - \frac{1}{\widehat{\mathrm{R}}\,\mathrm{ePr}}\Delta_f\theta\right) + \frac{1}{h^2}\left(\frac{1}{r}\frac{\partial\psi}{\partial x}\cdot\frac{\partial\theta_R}{\partial r} + \frac{1}{\widehat{\mathrm{R}}\,\mathrm{ePr}}\Delta_f\theta_R\right) \tag{39}$$

By projecting (35) in the Galerkin basis $\left(q_i(x)p_{2j}(r)\right)_{ij}$, one obtains at each time step a system of linear equations solved by the classical Gauss method.

One can notice that the use of Chebyshev polynomials in both axial and radial directions is not obvious, and contribute to emphasize this numerical method.

7. Convective heat transfer

The local convective heat transfer coefficient h_T is written as follows:

$$h_T(x, t) = \frac{\Phi_W}{\Delta T_{ref}} \tag{40}$$

where ΔT_{ref} is a typical difference temperature reference. That one depends on the wall boundary conditions hypotheses.

We have chosen:

$$\Delta T_{ref}(x, t) = T_W - T_m(x, t), \tag{41}$$

where $T_m(x, t)$ is the mean bulk temperature given by:

$$T_m(x, t) = \frac{\int_0^1 u(x, r, t).T(x, r, t).rdr}{\int_0^1 u(x, r, t).rdr} \tag{42}$$

The instantaneous convective heat transfer in unsteady flows can formally be defined by the local Nusselt number $Nu(x, t)$, given by the relation:

$$Nu(x, t) = \frac{Rh_T(x, t)}{k} \tag{43}$$

With the variables transform given in section 4, the Nusselt number can be written as follows:

$$Nu(x, t) = \frac{1}{h\lambda}\sqrt{\lambda^2 + h'^2}\,\frac{(\partial\theta(x, t)/\partial r)_W}{1 - \theta_m(x, t)} \tag{44}$$

where h' is the derivative oh the function h.

8. Numerical results

8.1 Definition of geometrical, physical and numerical parameters

8.1.1 Geometrical and physical parameters. The studied fluid is air, under normal conditions of temperature and pressure. The fluid flow is submitted to a pure sinusoidal pulsation. The previous studies (André *et al.*, 1981, 1987) showed that the numerical results are in the more stable mode if the ratio R/L is small, compared to the unit. Consequently, the basic geometry parameters are:

$$R = 0{,}02 \text{ m}; L = 0{,}08 \text{ m}; e = \frac{E}{R} = 2, R_V = 3R = 0{,}06 \text{ m}.$$

The sinusoidal surface of the wall is represented by the function h:

$$h(x) = 1 + \frac{e}{2}[1 - \cos(\pi . n_O(x + 1))] \tag{45}$$

where n_O indicates the number of geometrical periods chosen here equals to 3.

8.1.2 Choice for the orders of truncature. To ensure the accuracy of our results from the numerical point of view, we try several orders of truncature in the Chebyshev basis developments (see Batchi (2005) for details). When the orders of truncature increase, let $e_{\alpha\beta}$ be the error calculated between two consecutive truncature orders α and β of the stream function coefficients ψ_{kl} (respectively, the temperature coefficients θ_{kl}) relative to the steady flow.

The expression of $e_{\alpha\beta}$ is:

$$e_{\alpha\beta} = \max_{k,l} \left| f_{kl}^{\alpha} - f_{kl}^{\beta} \right| \tag{46}$$

where f^{α} represents ψ or θ, for the truncature order α.

Numerical study according to Nx and Nr parameters. For the dynamic point of view, we note first that the truncature errors $e_{\alpha\beta}$ depend mainly on the parameter Nx. This means that the increase in the number of polynomials in the radial direction does not improve the convergence of the results. Second, Figure 2 shows that the amplitudes of $e_{\alpha\beta}$ decrease when the values of Nx increase. With Nr fixed to 5 and $Nx \geq 30$, the truncature errors $e_{\alpha\beta}$ are negligible, about 2.10^{-4}.

Numerical study according to Mx and Mr parameters. For a given value of Mr, we observe in Figure 3 a good convergence of the temperature coefficients when Mx increases. But, unlike dynamic field, for the range of Mr values between 5 and 9, the analysis of the thermal field leads to slightly different conclusions. Indeed, probably due to the temperature conditions imposed on the entry section, the thermal field is more sensitive to the parameter Mr than dynamic field. For a fixed value of Mx, the temperature truncature errors increase with Mr. Then, optimal convergence is obtained for $Mr = 5$. For this value, the truncature error is less than 10^{-8} when $Mx > 56$.

In conclusion, we have selected for the dynamic problem: $Nx = 30$ and $Nr = 5$, and for the thermal problem, we have chosen: $Mx = 120$ and $Mr = 5$.

8.2 The steady flow

8.2.1 Study of the dynamic field. In order to study the dynamic behaviour of the flow according to the flow-rate, we varied the Reynolds number between 1 and 50. Figure 4 shows that the flow remains "with parallel lines", i.e. of crawling type, until $Re = 8$. From this value, a vortex initially appears in the first geometrical period, with a center shifted upstream and close to the wall. Then, when Re increases, a less bulky vortex

appears in the two other geometrical periods. The center of each vortex moves towards the downstream while moving away from the wall more and more gradually. The respective volumes occupied by the second and the third vortex and their relative positions within the undulation are almost identical. These results perfectly agree with those previously shown by Blancher (1991) and Batina *et al.* (2004).

8.2.2 Thermal study. Figure 5 shows a comparative study of the convective heat transfer by means of the Nusselt number, in stationary regime. Different geometries have been studied: tubes of sinusoidal surface, circular cylindrical tube of radius R. One can clearly see that the vortex has a negative influence on the heat transfer on almost

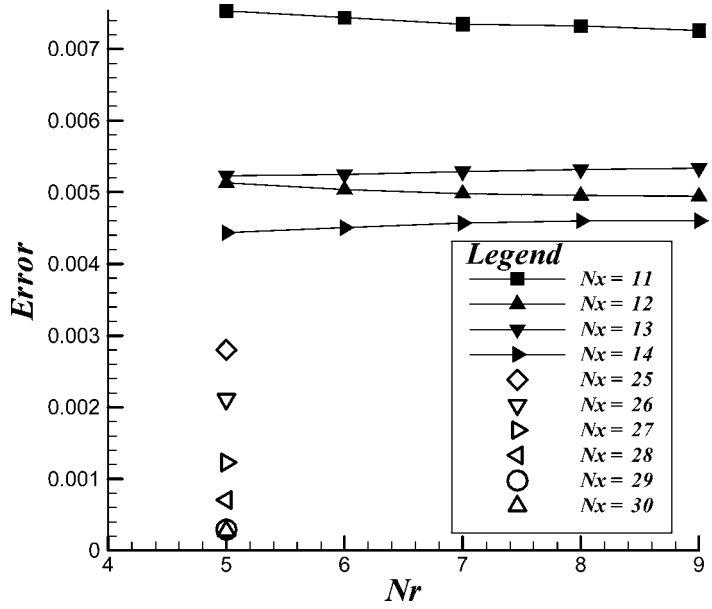

Figure 2.
Maximum truncature error in the Chebyshev basis development of the stream function ψ (steady flow, $Re = 30$)

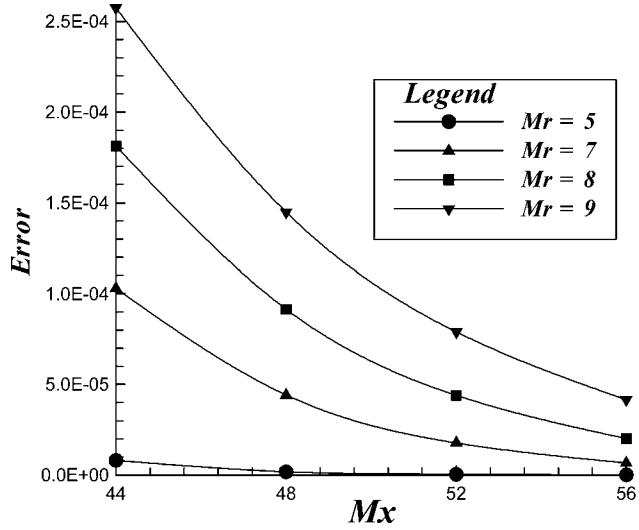

Figure 3.
Maximum truncature error in the Chebyshev basis development of the temperature function θ (steady flow, $Re = 30$)

the totality of the duct, except for the entry. Locally, we observe a light heat transfer enhancement at the constriction which increases with the amplitude of geometry.

From this parametric study, we can give the following conclusions:

(1) The presence of the undulations causes the apparition of vortex in the furrow beyond a critical Reynolds number equal to 8.

(2) The size of these vortices increases with Re until they fill the totality of the furrow.

(3) In this type of geometry, the spatial periodicity of the flow seems reached only at the end of the second furrow, even the third. The dynamic phenomena are of higher amplitudes in the first undulation due to the proximity of the duct entry. Thus one can expect substantial modifications on the heat transfer in this privileged area as previously shown by Batina *et al.* (1989, 1991).

8.3 Unsteady flow

In order to maintain the bidimensional hypothesis, the flow is submitted to low frequencies ($0 \leq f \leq 5$ Hz) and the amplitude of pulsation τ do not exceed 70 per cent. The Reynolds number is fixed to 30 corresponding to a total filling of the furrows.

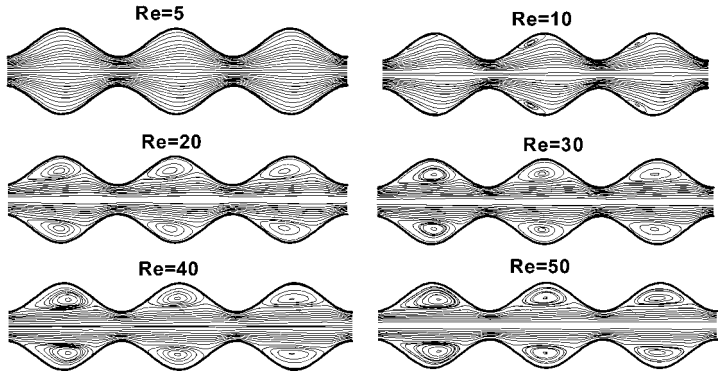

Figure 4.
Parametric study vs Reynolds number for three spatial cells

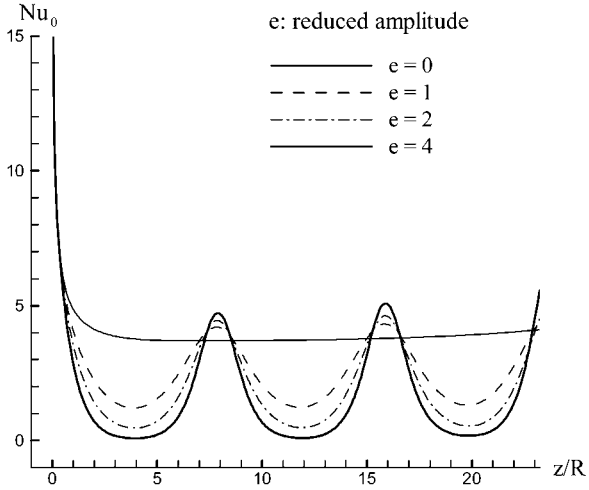

Figure 5.
Heat transfer comparison (steady case): different cylindrical tubes with sinusoidal surface; parametric study according to the reduced amplitude e of the geometry

However one will notice that the present bidimensional hypothesis is a first stage toward a survey of a 3D problem stability. The corresponding steady regime is taken as initial condition for the unsteady mode (instant $t = 0$).

To understand the fluid dynamic behaviour in pulsed regime, Figure 6 shows the detail of the streamlines for one period T. We note that the vortices quickly disappear

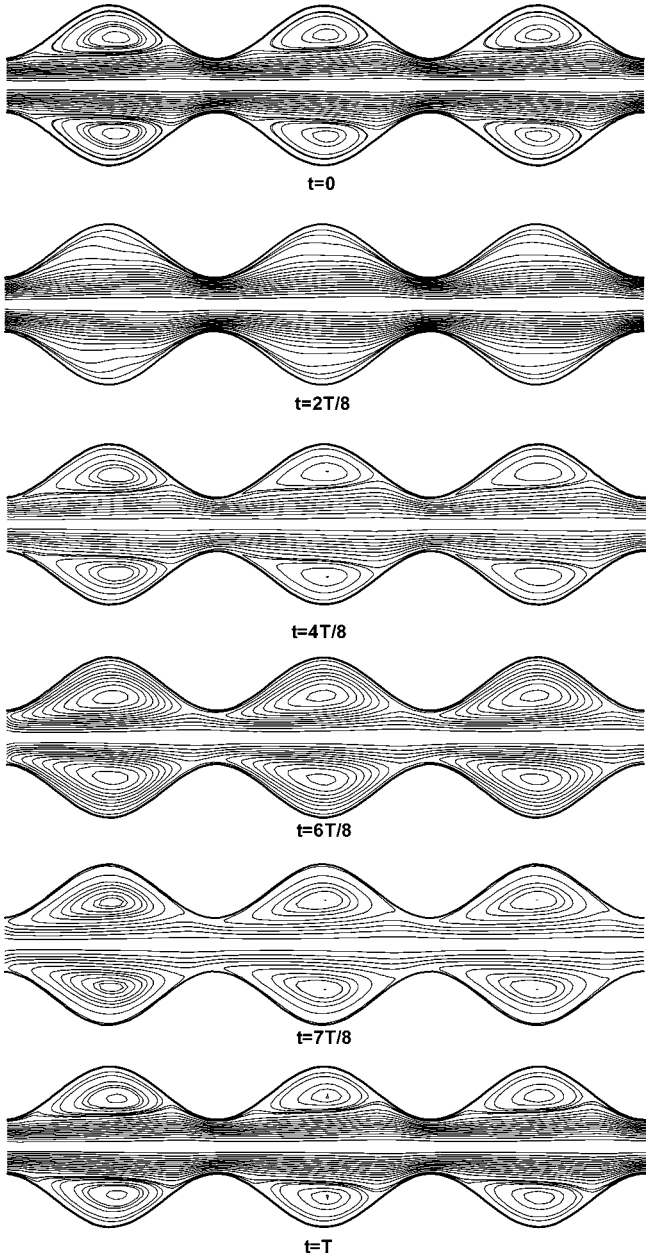

Figure 6.
Time history streamlines during one period, $\Omega = 0.3$, $Re = 30$, $Pr = 0.73$, $\tau = 0.7$

during the first instants, from $t = T/8$ to $t = 3T/8$. This interval of time corresponds to the phase of the flow acceleration, with a maximum reached for $t = T/4$. After that, a phase of deceleration appears, with a passage to zero for $t = T/2$. The size of the vortex is maximal for $t = 3T/4$. This stage corresponds to the maximum of the flow deceleration ($\Omega t = 3\pi/2$). In the central zone, the flow moves in positive direction, and close to the wall, the flow moves in opposite direction. After this, the fluid moves more closer to the wall. For the acceleration phase which follows, the flow tends to take its initial aspect again. However, with $t = T$, we approximately find the form of the flow for $t = 0$.

8.3.1 The velocity radial profiles. In order to study the radial profiles modifications, Figure 7 presents the temporal evolution of the radial profiles at different sections along the duct. One notes the presence of a light annular effect near the tube constriction (Batina *et al.*, 1989, 1991; Cebeci, 1973). Moreover, the profile corresponding to $t = 3T/4$ shows clearly the presence of a backward flow with high amplitude gradient in the vicinity of the wall. The amplitude of this phenomenon gradually increases during the phase of the flow deceleration.

8.3.2 Temporal evolution of the unsteady temperature field. Particular control points are located in the duct as shown in Figure 8. These points are chosen because we expect significant results on dynamical and thermal phenomena in this region.

To understand the thermal fluid response to the periodic solicitations imposed to the flow, Figure 9 presents the temporal evolution of the unsteady temperature at the

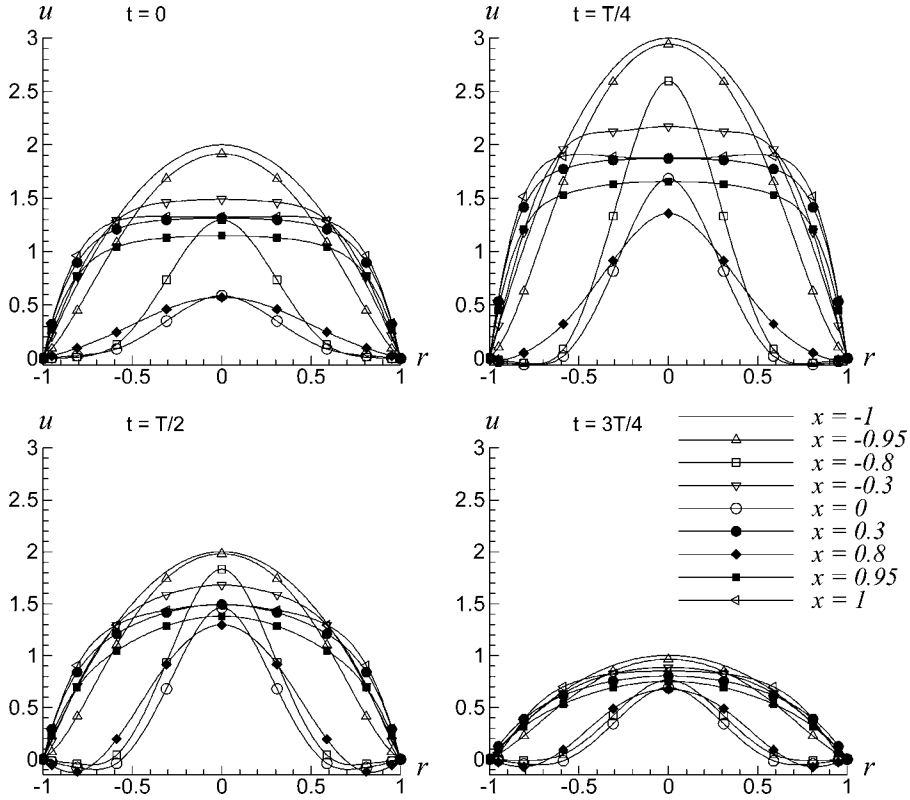

Figure 7.
Temporal evolution of the radial profiles at different times and sections along the duct, $\Omega = 0.3$, $Re = 30$, $Pr = 0.73$, $\tau = 0.5$

control points, indicated in Figure 8. We observe that this evolution is far from being uniform in the whole fluid vein. Indeed, in the immediate entry vicinity and close to the wall, the fluid temperature follows the imposed periodic solicitations after a transient stage, the duration of which depends on the position of the point.

The transient phase is as shorter as the point is near the source of pulsations and closed to the axis. Beyond this transient phenomenon, we have a permanent regime and the temporal evolution at all points seems perfectly sinusoidal. We notice that the temperature amplitudes of each point depend on its duct position.

In order to have a global vision of the dynamic and thermal unsteady phenomena, we carried out a spectral analysis with the FFT method, for the velocity and temperature fields, on three temporal periods ($t > 10$). The Figures 10 and 11 show that the most significant dynamic fluctuations are located at each constriction tube for axial velocities and downstream the constriction for radial velocities. One can thus expect a substantial modification of the thermal convective heat transfer in these privileged areas, due to the thermal boundary modifications corresponding to the entry section duct, and in the minimum sections as shown in Figure 5.

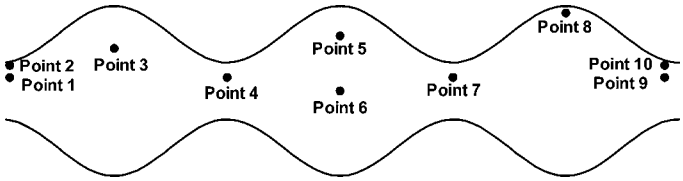

Figure 8.
Localization of control points for the description of the time-history phenomena

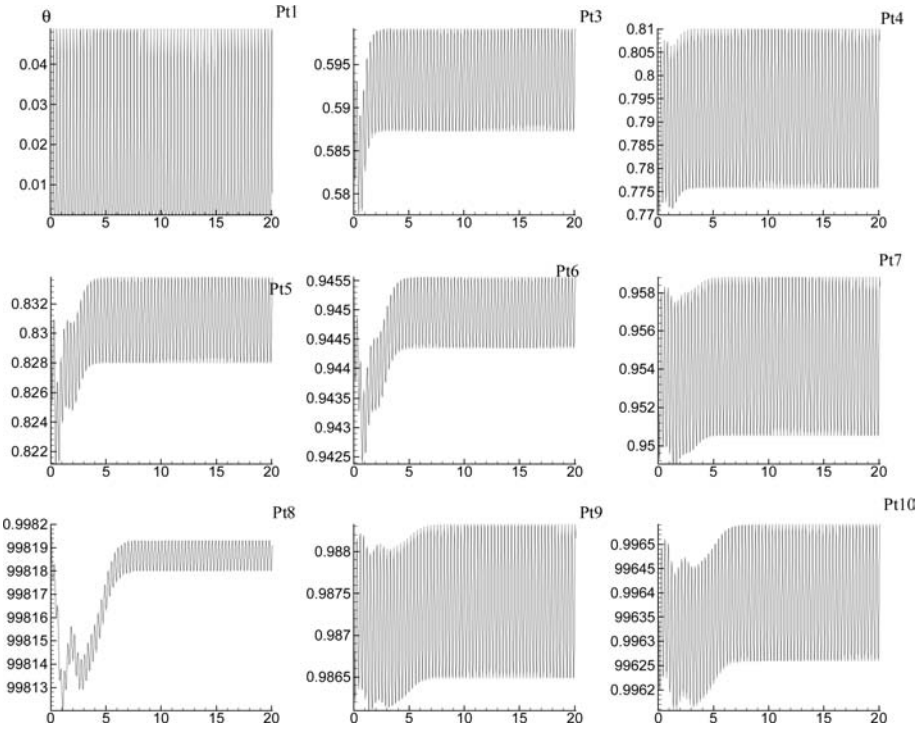

Figure 9.
Temporal evolution of the unsteady temperature to the points of control indicated on Figure 8. $Re = 30$, $Pr = 0.73$, $\tau = 0.7$

8.4 Unsteady convective heat transfer

On Figure 12, we study the Nusselt number evolution vs Ω, the pulsation frequency located at point 4. This amplitude analysis is obtained by the FFT method realised on the instantaneous Nusselt number defined by Equation (44). We observe a maximum for the Nusselt number amplitudes for $\Omega = 0.3$.

The instantaneous heat transfer does not correspond to a measurable physical reality. Thus it is necessary to consider the time averaged Nusselt number to quantify the local heat transfer in this particular study:

$$\overline{Nu}(x) = \langle Nu(x,t) \rangle = \frac{\omega}{2\pi} \int_0^{2\pi/\omega} Nu(x,t)dt \tag{47}$$

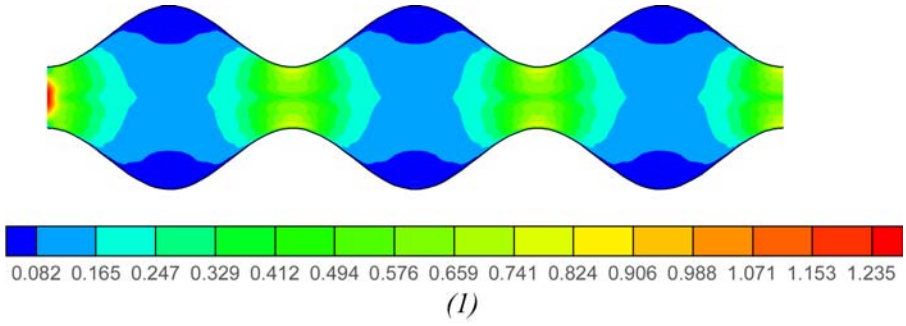

Figure 10.
Amplitudes fluctuations for the axial (1) and radial (2) velocity. $Re = 30$, $\tau = 0.7$

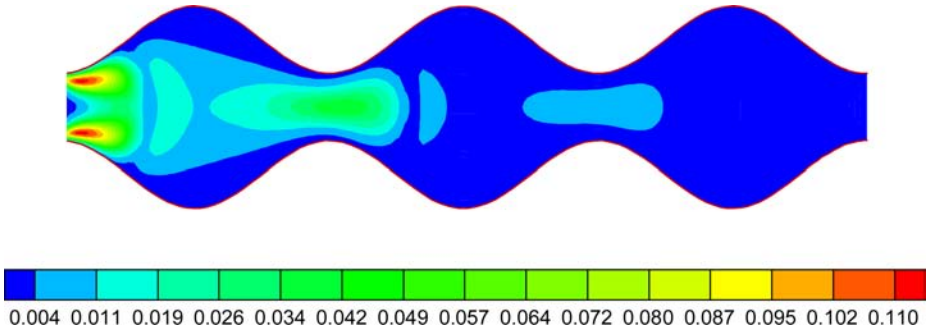

Figure 11.
Amplitudes fluctuations of the temperature. $Re = 30$, $Pr = 0.73$, $\tau = 0.7$

To evaluate the contribution of the pulsation on the heat transfer, we compare $\overline{Nu}(x)$ with the Nusselt number Nu_0 *(x)* obtained in steady flow. We confirm in Figure 13, a very significant increase of the heat transfer located at the constriction, and conversely a high reduction at maximum radius areas (zones of dead fluid). It is also noticed that the values of the Nusselt number in stationary regime are higher than those obtained in non-stationary mode, particularly at constriction regions.

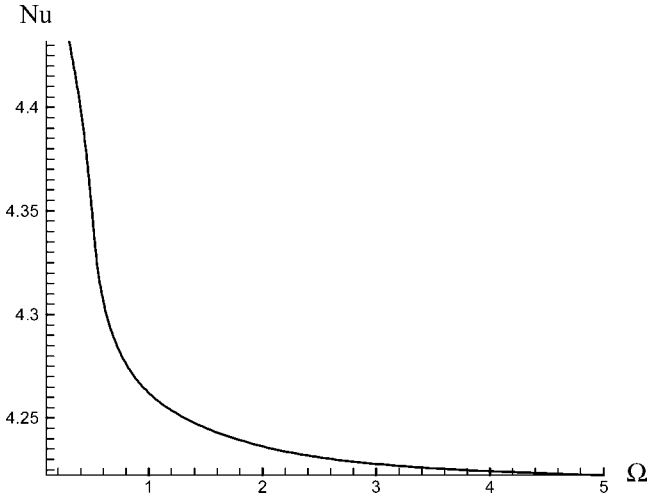

Figure 12.
Evolution of Nusselt number with pulsation frequency on the item 4, $Re = 30$; $Pr = 0.73$; $\tau = 0.7$

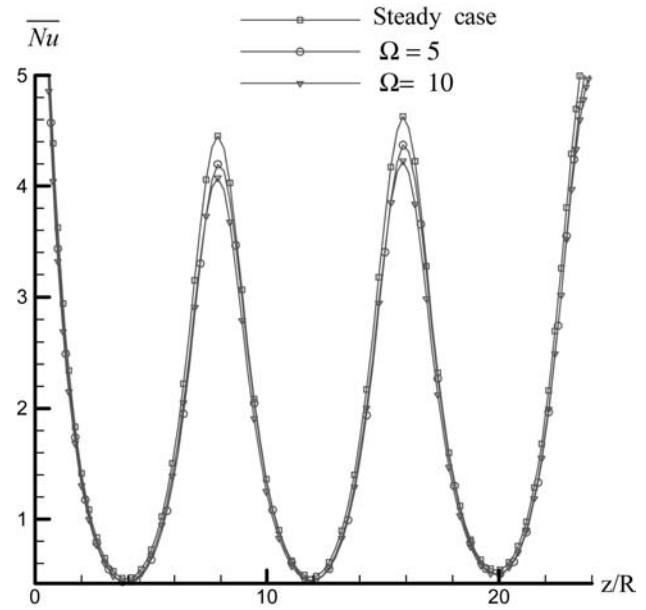

Figure 13.
Heat transfer comparison in steady and unsteady flow ($\Omega = 10$, $\Omega = 5$, $\tau = 0.7$)

9. Conclusions

The previous numerical results with low pulsations have shown that the heat transfer modification in cylindrical axisymmetric geometries is generally negligible, except for the duct entry (Batina *et al.*, 1989, 1991). At this section and close to the wall, important thermal effects are observed. In this paper, numerical studies have been carried out on pulsating flows through axisymmetric sinusoidal ducts. Thus, the study emphasizes on the heat transfer modifications in this particular flows with rates modulation close to the unit. The results obtained have shown that the flow in the axisymmetric geometry is influenced by many parameters including Reynolds numbers, rate modulation and amplitude of geometry. We observe that the results are encouraging and offer good perspectives in pulsed internal flows cases. From numerical point of view, the results obtained confirm the previous general conclusions in axisymmetric geometries (André *et al.*, 1981, 1987; Batina *et al.*, 1989, 1991), i.e.:

(1) For the steady regime: all classical results are obtained with high precision.

(2) For the unsteady regime, dynamic and thermal fields show an important heat transfer enhancement in the entry zone. A dynamic and thermal shock occur nearly this area. Mechanical tube behaviour can be modified in this region and the shear stress occurring during the pulsation can induce some damage if the tube is connected to a big tank. This phenomenon is of great interest in industrial structures. Nevertheless, convective heat transfer decrease when the fluid moves forward in the tube.

Out of these general conclusions, this study focusing on sinusoidal geometries induce especially zones of dead fluid that locally have a negative influence on heat transfer, particularly for the steady flow. The spatial periodicity of the steady flow in this type of geometry is acquired only at the end of the second, even third geometrical period. The transient phenomena are therefore relatively short in time. Thus, the dynamic and thermal behaviours of the flow become periodic.

Compared to models based on classical methods such as asymptotic developments, finite differences, finite volumes, finite elements, etc, our numerical method leads to the following remarks:

(1) The accuracy of the present model is high.

(2) The present computational code is easier to build compared to finite elements one, for example.

(3) If we consider the CPU time, the present model needs few minutes to compute the numerical equations. This result traduces the efficiency of our model which is easier and more adapted to solve this particular problem. Nevertheless, compared to some industrial code, our model have some disadvantages, such as:

- the non-linear coupled unsteady terms in Navier-Stokes and energy equations are not taken into account in the present model;
- this problem require smoother geometries;
- the order of polynomials developments increases strongly the computing time;
- when the modulation flow-rate approaches the unity, we must choose carefully some data to assume the algorithms convergence. For example,

when $\tau > 100$ per cent, convergence conditions impose small time steps, and the CPU time on classical computers can make our code prohibitive.

In a final analysis, our numerical method based on a suitable spectral method is of a good accuracy. One of its originality is the choice of Chebyshev polynomials basis in both axial and radial directions, and the use of a shift operator technique allow the introduction of non-homogeneous boundary conditions. The automatic construction of these polynomials is of a great interest. These particular mathematical and numerical tools have permitted the resolution of this non-obvious problem which consists on pulsated unsteady flows associated to simultaneous developments dynamic and thermal fields.

References

André, P., Creff, R. and Batina, J. (1981), "Etude des conditions particulières de fréquence favorisant les transferts thermiques en écoulements pulsés en canalisation cylindrique", *International Journal of Heat and Mass Transfer*, Vol. 24, pp. 1211-19.

André, P., Creff, R. and Batina, J. (1987), "Study of thermal fluid for pulsed flow with compressible fluids", Numerical Methods in Thermal Problems, Fifth International Conference, Montreal, Canada, Pineridge Press, Swansea, pp. 149-54.

Batchi, M. (2005), "Etude Mathématique et Numérique des Phénomènes de Transferts Thermiques liés aux Ecoulements Instationnaires en Géométrie Axisymétrique", Thèse de Doctorat Mathématiques Appliquées, Université de Pau, Pau.

Batina, J. (1995), "Etude numérique des écoulements instationnaires pulsés en canalisation cylindrique", Thèse de Doctorat Physique, Université de Pau, Pau.

Batina, J., Creff, R. and Batchi, M. (2004), "Etude thermique convective d'un écoulement interne en géométrie axisymétrique sinusoïdale", *Actes du congrès SFT 04*, pp. 987-92.

Batina, J., André, P., Creff, R. and Blancher, S. (1991), "Dynamic and thermal developments of a pulsed laminar compressible ducted flow", *Proceedings Eurotherm*, *Pau*, No. 25, pp. 227-34.

Batina, J., Creff, R., André, P. and Blancher, S. (1989), "Numerical model for dynamic and thermal developments of a turbulent pulsed ducted flow", *Proceedings Eurotherm*, *Bochum*, No. 9, pp. 50-7.

Bernardi, C. and Maday, Y. (1992), *Approximations Spectrales De Problèmes Aux Limites Elliptiques*, Springer-Verlag, France.

Blancher, S. (1991), "Transfert convectif stationnaire et stabilité hydrodynamique en géométrie périodique", Thèse de Doctorat Physique, Université de Pau, Pau.

Canuto, C., Hussaini, M.Y., Quarteroni, A. and Zang, T.A. (1988), *Spectral Methods in Fluids Dynamics*, Springer-Verlag, New York, NY.

Cebeci, T. (1973), "A model for eddy conductivity and turbulent Prandtl number", *International Journal of Heat and Mass Transfer*, Vol. 95, pp. 227-34.

Chakravarty, S. and Sannigrahi, A.K. (1999), "A nonlinear mathematical model of blood flow in a constricted artery experiencing body acceleration", *Mathematical and Computer Modeling*, Vol. 29, pp. 9-25.

Creff, R., Batina, J. and André, P. (1985), "A numerical model for a pulsed laminar flow with slightly compressible fluid", Numerical Methods in Laminar and Turbulent Flow, Fourth International Conference, Pineridge Press, Swansea, pp. 63-72.

Fedele, F., Hitt, D.L. and Prabhu, R.D. (2005), "Revisiting the stability of pulsatile flow", *European Journal of Mechanics and fluids*, Vol. 24, pp. 237-54.

Ghaddar, N.K., Magen, M., Mikic, B.B. and Patera, A. (1986), "Numerical investigation of incompressible flow in grooved channels, resonance and oscillatory heat transfer enhancement", *Journal of Fluid Mechanics*, Vol. 168, pp. 541-67.

Gelfgat, A.Y. (2004), "Stability and slightly supercritical oscillatory regimes of natural convection in a 8:1 cavity: solution of the benchmark problem by a global Galerkin method", *International Journal of Numerical Methods in Fluids*, Vol. 44, pp. 135-46.

Guo-Tao, L., Xian-Ju, W., Bao-Quan, A. and Liang-Gang, L. (2004), "Numerical study of pulsating flow through a tapered artery with stenosis", *Chinese Journal of Physics*, Vol. 42 No. 4-I, pp. 401-6.

Gurek, C., Guleren, K.M., Aydin, K. and Pinarbasi, A. (2002), "Steady laminar flow computation through vascular tube constrictions", *Proceedings of the 6th Biennial Conference on ESDA, Bio-010*, pp.1-7.

Hemida, H.N., Sabry, M.N., Abdel-Rahim, A. and Mansour, H. (2002), "Theoretical analysis of heat transfer in laminar pulsating flow", *International Journal of Heat and Mass Transfer*, Vol. 45, pp. 1767-80.

Lee, B.S., Kang, L.S. and Lim, H.C. (1999), "Chaotic mixing and mass transfer enhancement by pulsatile laminar flow in an axisymmetric wavy channel", *International Journal of Heat and Mass Transfer*, Vol. 42, pp. 2571-81.

Moschandreau, T. and Zamir, M. (1997), "Heat transfer in a tube with pulsating flow and constant heat flux", *International Journal of Heat and Mass Transfer*, Vol. 40 No. 10, pp. 2461-66.

Ryval, J., Straatman, A.G. and Steinman, D.A. (2003), "Low Reynolds number modeling of pulsatile flow in a moderately constricted geometry", *Proceedings of the 11th Annual Conference of the CFD Society Of Canada*, Vol. 1, pp. 300-4.

Shen, J. (1994), "Efficient spectral-Galerkin method I: direct solvers for the second and fourth order equations using Legendre polynomials", *SIAM Journal of Scientific Computing*, Vol. 15 No. 6, pp. 1489-505.

Shen, J. (1995), "Efficient spectral-Galerkin methods II: direct solvers of second and fourth order equations by using Chebyshev polynomials", *SIAM Journal of Scientific Computing*, Vol. 16 No. 8, pp. 74-87.

Shen, J. (1997), "Efficient spectral-Galerkin methods III: polar and cylindrical geometries", *SIAM Journal of Scientific Computing*, Vol. 18 No. 6, pp. 1583-604.

Young Kim, S., Ha Kang, B. and Min Hyun, J. (1998), "Forced convection heat transfer from two heated blocks in pulsating channel flow", *International Journal of Heat and Mass Transfer*, Vol. 41 No. 3, pp. 625-34.

Further reading

Charalampos, K. and Tsamopoulos, J. (2000), "Concentric core-annular flow in a circular tube of slowly varying cross-section", *Chemical Engineering Science*, Vol. 55, pp. 5509-30.

Sobey, I.J. (1980), "On flow through channels. Part 1: calculated flow patterns", *Journal of Fluid Mechanics*, Vol. 96, pp. 1-26.

Uchida, S. (1956), "The pulsating viscous flow superposed on the steady laminar motion of uncompressible fluid in a circular duct", *Zeitschrift für angewandte Mathematik und Physik*, Vol. 7, pp. 403-22.

Zhixiong, G. and Hyung Jin, S. (1997), "Analysis of the Nusselt number in pulsating pipe flow", *International Journal of Heat and Mass Transfer*, Vol. 40 No. 10, pp. 2486-9.

Corresponding author

J. Batina can be contacted at: jean.batina@univ-pau.fr

To purchase reprints of this article please e-mail: **reprints@emeraldinsight.com**
Or visit our web site for further details: **www.emeraldinsight.com/reprints**